International Journal of Radiation Oncology biology • physics

www.redjournal.org

Physics Contribution

Water Exchange Rate Constant as a Biomarker of Treatment Efficacy in Patients With Brain Metastases Undergoing Stereotactic Radiosurgery

Hatef Mehrabian, PhD,[*,†] Kimberly L. Desmond, PhD,[†] Sofia Chavez, PhD,[‡] Colleen Bailey, PhD,[§] Radoslaw Rola, MD, PhD,[‖] Arjun Sahgal, MD,[†,¶] Gregory J. Czarnota, PhD, MD,[*,†,¶] Hany Soliman, MD,[¶] Anne L. Martel, PhD,[*,†] and Greg J. Stanisz, PhD[*,†,‖]

Medical Biophysics, University of Toronto, Toronto, Ontario, Canada; †Physical Sciences, Sunnybrook Research Institute, Toronto, Ontario, Canada; ‡Research Imaging Centre, Centre for Addiction and Mental Health, Toronto, Ontario, Canada; §Computer Science Department, University College London, London, United Kingdom; ‖Neurosurgery and Pediatric Neurosurgery, Medical University, Lublin, Poland; and ¶Radiation Oncology, Sunnybrook Health Sciences Centre, Toronto, Ontario, Canada

Received Sep 9, 2016, and in revised form Dec 12, 2016. Accepted for publication Jan 2, 2017.

Summary

Cells undergoing apoptosis experience an increased intracellular to extracellular water exchange rate. A water exchange quantification technique for clinical DCE-MRI was developed and applied to 19 brain metastases patients treated with stereotactic radiosurgery (SRS). The intra−extracellular water exchange rate

Purpose: This study was designed to evaluate whether changes in metastatic brain tumors after stereotactic radiosurgery (SRS) can be seen with quantitative MRI early after treatment.

Methods and Materials: Using contrast-enhanced MRI, a 3-water-compartment tissue model consisting of intracellular (I), extracellular-extravascular (E), and vascular (V) compartments was used to assess the intra−extracellular water exchange rate constant (k_{IE}), efflux rate constant (k_{ep}), and water compartment volume fractions ($M_{0,I}$, $M_{0,E}$, $M_{0,V}$). In this prospective study, 19 patients were MRI-scanned before treatment and 1 week and 1 month after SRS. The change in model parameters between the pretreatment and 1-week posttreatment scans was correlated to the change in tumor volume between pretreatment and 1-month posttreatment scans.

Results: At 1 week k_{IE} differentiated ($P<.001$) tumors that had partial response from tumors with stable and progressive disease, and a high correlation ($R=-0.76$,

Reprint requests to: Hatef Mehrabian, PhD, Sunnybrook Research Institute, 2075 Bayview Ave, Room S6-05, Toronto, ON M4N 3M5, Canada. Tel: (416) 480-6100, ext. 2455; E-mail: hatef.mehrabian@sri.utoronto.ca

This study was funded by following grants: Terry Fox Research Institute (TFRI project 1034) and Canadian Cancer Society Research Innovation (CCSRI 701640).

Conflict of interest: none.

Supplementary material for this article can be found at www.redjournal.org.

Int J Radiation Oncol Biol Phys, Vol. 98, No. 1, pp. 47−55, 2017
0360-3016/$ - see front matter
http://dx.doi.org/10.1016/j.ijrobp.2017.01.016

identified partial response patients within 1 week after treatment and also predicted the extent of tumor shrinkage at 1 month. Thus, intra–extracellular water exchange rate is a promising biomarker of brain metastases response to SRS.

$P<.001$) was observed between early changes in the k_{IE} and tumor volume change 1 month after treatment. Other model parameters had lower correlation ($M_{0,E}$) or no correlation (k_{ep}, $M_{0,V}$).

Conclusions: This is the first study that measured k_{IE} early after SRS, and it found that early changes in k_{IE} (1 week after treatment) highly correlated with long-term tumor response and could predict the extent of tumor shrinkage at 1 month after SRS.

Introduction

Brain metastases have a significant impact on patient quality of life and survival. In the course of cancer illness up to 40% of patients develop brain metastases (1). Stereotactic radiosurgery (SRS) is a useful tool to treat brain metastases and has been found to improve patient outcomes, including survival, in patients with single metastases (2). Evaluation of tumor response to SRS is carried out using the Response Assessment in Neuro-Oncology-Brain Metastasis (RANO-BM) criteria (3) which relies on the changes in tumor size. However, it may take weeks or months before significant changes in tumor size take place. Moreover, early changes in tumor size do not always correlate with later outcomes (4), and very few studies have attempted (with limited success) to evaluate treatment response with quantitative MRI within a few days after treatment (5-7). Thus, more robust markers of response are desired that can quantify early molecular or cellular changes in the tumor, such as those seen in apoptosis (8, 9). Identifying nonresponders early after treatment and avoiding delays to salvage treatments may lead to better treatment outcomes.

Stereotactic radiosurgery induces DNA damage in tumor cells, which leads to programmed cell death (apoptosis). It has been shown in vitro (10) and in animal models (11) that cellular apoptosis can be detected by MRI (within 48 hours after treatment) through quantification of the water exchange rate constant between intracellular and extracellular compartments, k_{IE} (10-12). The water exchange rate increases in apoptotic cells owing to the increased surface-to-volume ratio of the cell either by transformation of the cell into a less spherical shape or decreased volume overall (10, 13) and, to lesser extent, owing to increased cellular membrane permeability to water molecules (10).

There exist several techniques to measure the water exchange rate constant between intracellular and extracellular compartments (11, 12, 14-17). Landis et al (18) and, more recently, Bailey et al (11) applied a 2-compartment tissue relaxation model to contrast-enhanced MRI with multiple injections of contrast agent (CA), to calculate water exchange rate. Multiple injections of CA make these techniques time-consuming and difficult to translate into clinic. Other approaches that can be more easily applied to the in vivo dynamic contrast-enhanced (DCE)-MRI have also been proposed. Yankeelov et al (17, 19) and Springer et al (14) use a 2-compartmental model of water exchange between the intracellular and extracellular compartments and incorporate a tracer kinetic model (Tofts-Kety model [20]) into the apparent longitudinal relaxation rate constant's measurement (while ignoring the contribution of the tumor's vascular compartment).

In the present study we use a modified approach for evaluating the intracellular to extracellular–extravascular water exchange rate constant from clinical DCE-MRI data using a combination of a 3 water compartment tissue model and a vascular signal separation technique called independent component analysis (ICA). The ICA-based separation (21-24) provides the MRI signal of vascular and extracellular–extravascular compartments using the standard, clinically used DCE-MRI datasets and yields sufficient signal measurement to fit to the water exchange model.

The focus of this study was to evaluate this novel imaging approach as an early biomarker of tumor response to SRS. We hypothesized that shortly after SRS, the intra–extracellular water exchange rate constant, which is a surrogate of tumor apoptosis, can differentiate between responders and nonresponders.

Methods and Materials

Three-pool relaxation model

Each voxel in DCE-MRI was assumed to be composed of 3 water compartments: vascular (V), extracellular–extravascular (E), and intracellular (I), and a 3-water-compartment relaxation model (Fig. 1) was used. Each compartment in a voxel was assumed to contain a fraction of the voxel's total water content proportional to its volume fraction ($M_{0,V}$, $M_{0,E}$, $M_{0,I}$). Water was assumed to transfer from the intracellular, I, to extracellular–extravascular compartment, E, with exchange rate constant, k_{IE}. The water exchange between vascular, V, and extracellular–extravascular, E, compartments was assumed to be negligible ($k_{VE} = k_{EV} = 0$). Detailed description of the

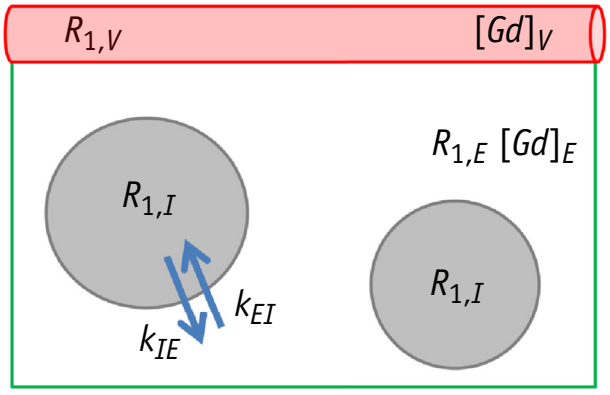

Fig. 1. Schematic of the 3-water-compartment model with water exchange across cell membrane. $[Gd]_V$ and $[Gd]_E$ represent contrast agent concentration in vascular and extracellular–extravascular compartments, respectively. R1,V, R1,E, and R1,I represent the longitudinal relaxation rates of each compartment. Water exchange rate constant from I to E compartment is described by exchange rate constant k_{IE}.

model and its mathematical formalism are presented in Supplementary-A (available online at www.redjournal.org).

The relationship between the measured MRI signal, S, and the 3-pool model parameters can be derived from Bloch-McConnell equations (25) and for a spoiled gradient echo sequence is given by:

$$S = S_0 \sin(f_{acc}\alpha)\left(M_{0,A}\frac{1-e^{-TR.R_{1,A}}}{1-\cos(f_{acc}\alpha)e^{-TR.R_{1,A}}} + M_{0,B}\frac{1-e^{-TR.R_{1,B}}}{1-\cos(f_{acc}\alpha)\,e^{-TR.R_{1,B}}} + M_{0,V}\frac{1-e^{-TR.R_{1,V}}}{1-\cos(f_{acc}\alpha)e^{-TR.R_{1,V}}}\right) \quad (1)$$

where S_0 is the equilibrium MRI signal, α is flip angle, f_{acc} is a correction factor for B_1 inhomogeneities, TR is repetition time, $R_{1,V}$ is the longitudinal relaxation rate of vascular compartment, the 2 apparent coefficients $M_{0,A}$ and $M_{0,B}$ are apparent volume fraction coefficients, and $R_{1,A}$ and $R_{1,B}$ are apparent rate constants (details defined in Supplementary-A; available online at www.redjournal.org).

Calculating the model parameters using Equation 1 requires knowing the CA concentration in the vascular and extracellular–extravascular compartments (assuming intracellular CA concentration is zero). A data-driven technique that is hereby called adaptive kernel independent component analysis (AK-ICA) was used to separate the MRI signal enhancement in the vascular and extracellular–extravascular compartments (21-24) (details of the AK-ICA technique are provided in Supplementary-B; available online at www.redjournal.org). Using AK-ICA to separate the signal enhancement in the vascular space enables obtaining all required information locally from the DCE-MRI of the tumor. Thus, arterial input function (AIF) calculation and its associated problems (ie, issues in the AIF measurement, bolus dispersion between the AIF measurement site and tumor, and difference between arrival time of the CA in the tumor and the AIF measurement site) are avoided (11, 16, 17, 19).

Figure 2 shows a sample DCE-MRI image of a patient with brain metastasis that was used in this study, as well as the rectangular region of interest (ROI) around the tumor (green rectangle) that was selected for AK-ICA analysis. The CA concentration in the extracellular–extravascular compartment was related to the vascular CA concentration with (extended Tofts-Kety model [26]):

$$[Gd]_E(t) = k_{ep}\int_0^t [Gd]_p(t)\exp\left(-k_{ep}(t-\tau)\right)d\tau \quad (2)$$

where $[Gd]_p = [Gd]_V/Htc$. $[Gd]_p$, $[Gd]_V$, and $[Gd]_E$ are the plasma, vascular, and extracellular–extravascular CA concentrations, respectively, Htc is the hematocrit level (assumed to be 0.42), and k_{ep} is the efflux rate constant ($k_{ep} = K^{trans}/M_{0,E}$, where K^{trans} is the volume transfer rate constant).

Model fitting

The longitudinal relaxation rate constants of vascular and extracellular–extravascular compartments in the presence of CA were assumed to be:

$$R_{1,V} = R_{10,V} + r_1[Gd]_V$$
$$R_{1,E} = R_{10,E} + r_1[Gd]_E \quad (3)$$

where $r_1 = 4.5\ \mathrm{mM^{-1}s^{-1}}$ at 3T for gadobutrol (27) and $R_{10,X}$ was the precontrast longitudinal relaxation rate constant of each compartment. $R_{10,V}$ was assumed to be equal to $0.61\ \mathrm{s^{-1}}$ (at 3T and with $Hct = 0.42$) (28). It was also assumed that the precontrast longitudinal relaxation rates of the extracellular–extravascular and intracellular compartments were equal ($R_{10,E} = R_{10,I}$) and these compartments were in fast exchange limit with vascular compartment before contrast administration (12, 29). Thus, $R_{10,E}$ was related to the precontrast longitudinal relaxation rate constant of the entire voxel (R_{10}) with:

$$R_{10,E} \equiv R_{10,I} \triangleq \frac{R_{10} - M_{0,V}R_{10,V}}{1-M_{0,V}} \quad (4)$$

The relaxation model therefore had 4 independent parameters ($M_{0,V}$, $M_{0,I}$, k_{IE}, k_{ep}) for each voxel, which were calculated by fitting the relaxation model to the measured signal values through least squared difference minimization, as follows:

$$\Gamma(\theta) = \min\left\{\left\|\frac{S(t,\theta)}{S(0,\theta)} - \frac{\widehat{S}(t)}{\widehat{S}(0)}\right\|_2^2\right\} \quad (5)$$
$$s.t.\ M_{0,V} + M_{0,E} < 1\ \&\ 0 \le M_{0,V}, M_{0,E}\ \&\ 0 \le t \le T$$

where $\theta = [M_{0,V}, M_{0,E}, k_{IE}, k_{ep}]$, and T was the duration of DCE-MRI scan, S was the theoretical signal intensity calculated using Equation 1, and $\hat{S}$ was the measured DCE-

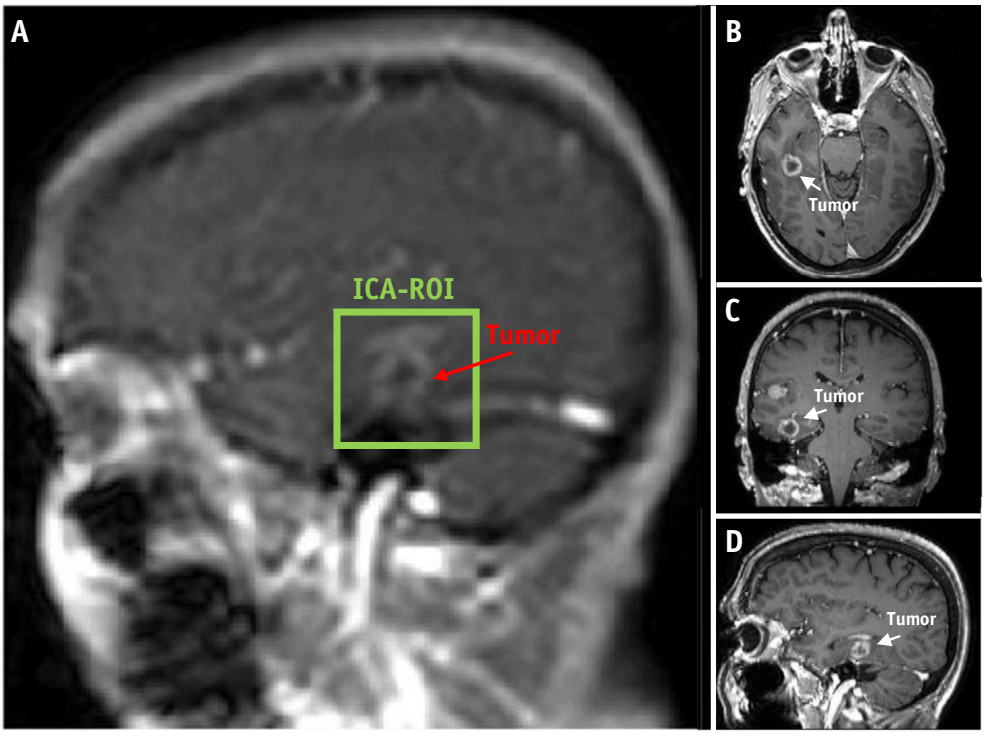

Fig. 2. (A) Gadolinium-enhanced T_1-weighted image (3.5 minutes after injection in dynamic contrast-enhanced MRI) in a patient with brain metastasis. The tumor can be detected as an enhancing region of interest in this image (red arrow). An area around the tumor (green rectangle) that was used in adaptive kernel independent component analysis (AK-ICA) and also relaxation modeling is also shown. (B) An axial cross section, (C) a coronal cross section, and (D) a sagittal cross-section of the brain showing the tumor, generated from 3-dimensional volume rendering of the high-resolution postcontrast axial T_1-weighted images. (A color version of this figure is available at www.redjournal.org.)

MRI signal intensity of the voxel. Chi-squared goodness of fit was evaluated using the chi2gof function in MATLAB (MathWorks, Natick, MA) and 5% significance level, and the voxels that failed this test were excluded from analysis.

Patient population

A total of 29 patients with metastatic brain tumors were recruited to investigate the predictive power of MRI in early assessment (1 week after treatment) of tumor response to SRS. Informed consent was obtained from all patients, and the study was conducted after research ethics board approval. Stereotactic radiosurgery involved delivering a single dose of 18 to 20 Gy radiation focally to the tumor using a linear accelerator–based SRS system. In this prospective study the patients were scanned at 3 time points: (*1*) before treatment (within 48 hours); (*2*) 3 to 10 days ("1 week") after treatment; and (*3*) 1 month after treatment. After the 1-month MRI scan all patients were followed with clinical MRI indefinitely to determine the treatment response and patient outcome.

Eight patients did not participate in the "1-week" follow-up scan and were excluded. One patient was excluded owing to the large motion during DCE-MRI acquisition, and 1 patient was excluded owing to difficulties in IV injection. Thus, DCE-MRI of 19 patients (1 tumor randomly selected for each patient) was analyzed in the study (clinical details listed in Table 1).

MRI acquisition

The patients were scanned on a 3T Philips Achieva MRI system (Best, the Netherlands) with 8-channel SENSE head coil with the following MRI sequences: DCE-MRI: sagittal, 3-dimensional (3D) fast field echo (FFE) with repetition time (TR)/echo time (TE) = 4 milliseconds/2.02 milliseconds, $\alpha = 15°$, field of view (FOV) = 25.6 cm × 25.6 cm, matrix = 256 × 256 × 20, slice thickness = 8 mm, temporal resolution = 5.2 seconds, number of time points = 60. A bolus of CA (Gadobutrol; Bayer, Toronto, Canada) was injected intravenously (0.1 mmol/kg of body weight followed by saline flush). The bolus injection was performed after acquisition of the third dynamic volume in the DCE-MRI sequence (approximately 15 seconds after the start of DCE-MRI acquisition).

The method of Slopes (MoS) was used for B_1 and R_1 mapping (30, 31) before administration of CA. The MoS imaging involved low spatial resolution images with large flip angles (FFE, $\alpha = 130°$,150°, TR/TE = 50 milliseconds/

Table 1 Clinical and MRI scanning details of the patients

Patient	Age (y)	Sex	Primary tumor	Treated tumors	Pre to SRS (d)	SRS to 1 wk (d)	Response (1 mo)	Response (long term)
P01	58	F	Lung	2	1	5	PR	Regression
P02	65	F	Endometrium	4	2	3	PR	Regression
P03	60	F	Thyroid	4	1	5	PD	Progression
P04	79	M	Lung	5	4	3	PR	Regression
P05	38	F	Breast	2	2	7	PR	Regression
P06	69	M	Lung	3	5	3	PD	Progression
P07	58	F	Breast	6	4	6	PR	Regression
P08	51	F	Breast	1	4	10	PD	Progression
P09	68	F	Lung	2	3	6	PR	Regression
P10	85	M	Rectum	1	1	5	PR	N/A
P11	77	F	Breast and lung	3	2	7	SD	Controlled
P12	48	F	Breast	11	2	8	PR	Regression
P13	57	M	Lung	1	0	7	PR	Regression
P14	75	F	Lung	1	3	6	SD	Controlled
P15	57	F	Breast	9	5	7	PR	N/A
P16	64	F	Lung	1	3	8	SD	Controlled
P17	80	F	Lung	2	4	8	PR	Regression
P18	65	F	Lung	3	1	7	PD	Progression
P19	51	F	Breast	2	3	10	PR	Progression

Abbreviations: PD = progressive disease; PR = partial response; RANO-BM = Response Assessment in Neuro-Oncology-Brain Metastasis; SD = stable disease; SRS = stereotactic radiosurgery.

Details shown include age, sex, primary tumor site, number of brain metastases treated with SRS (treated tumors), interval between pretreatment MRI scan and SRS (Pre to SRS), interval between SRS and 1-week posttreatment MRI scan (SRS to 1 wk), and the response assessment based on RANO-BM criteria (only 1 tumor per patient was studied).

5 milliseconds, FOV = 25.6 cm × 25.6 cm, matrix = 64 × 64 × 40, slice thickness = 4 mm) followed by high spatial resolution images with small flip angles (FFE, $\alpha = 3°,14°$, TR/TE = 10.7 milliseconds/5 milliseconds, FOV = 25.6 cm × 25.6 cm, matrix = 256 × 256 × 80, slice thickness = 2 mm). The large flip angle images were used for B_1 mapping. Then the low flip angle images and the B1 map were used for R_1 mapping.

Postcontrast 3D axial T_1-weighted imaging was also performed (TR/TE = 9.5 milliseconds/2.3 milliseconds, $\alpha = 8°$, FOV = 22 cm × 22 cm, matrix = 448 × 448 × 113, slice thickness = 1.5 mm) for tumor volume assessment. Dynamic contrast-enhanced MRI and axial T_1-weighted MRI were the last 2 sequences in the protocol, in which DCE-MRI was 5.2 minutes and 3D axial T_1-weighted MRI was approximately 7 minutes.

Data analysis

Tumor ROI on DCE-MRI was determined by subtracting the first image in the DCE-MRI series from the last image in the DCE-MRI series and then contouring the enhancing region. Model parameters were calculated for each voxel in this ROI. The average parameter value over ROI was then used in the figures and tables. The Wilcoxon rank sum test was used to determine statistical significance of the differences between parameter distributions before and 1 week after treatment. For each plot the Pearson correlation coefficient between the horizontal and vertical axes as well as the statistical significance of this correlation coefficient (calculated using a 2-tailed t test) were reported.

Tumor volume was determined by manually contouring the enhancing region on the high-resolution postcontrast T_1-weighted images. Tumor response was evaluated using RANO-BM (3) criteria. Among 19 patients, on the basis of tumor size measurements at 1 month after SRS, there were 12 patients with partial response (PR), 3 patients with stable disease (SD), and 4 patients with progressive disease (PD). The clinical outcomes of the patients were determined by considering the long-term follow-up of the patients (longer than 3 months) by an expert oncologist who was blinded to the analysis and results.

Results

The 3-pool relaxation model was applied to the pretreatment and 1-week posttreatment scans of all 19 patients, and the model parameters were calculated. Incorporation of the water exchange rate constant in the model equations added 1 extra parameter to the conventional tracer-kinetic models that ignore the water exchange rate constant. Adding the extra parameter to the model was warranted by F test and provided more accurate fit to the data and smaller residual and χ^2 values. Figure 3 shows the parametric maps of all 4 model parameters (k_{IE}, k_{ep}, $M_{0,V}$, $M_{0,E}$) for the case shown in Figure 2.

For each group of patients (PR, SD, PD), Table 2 reports the mean and standard deviation of change in each model

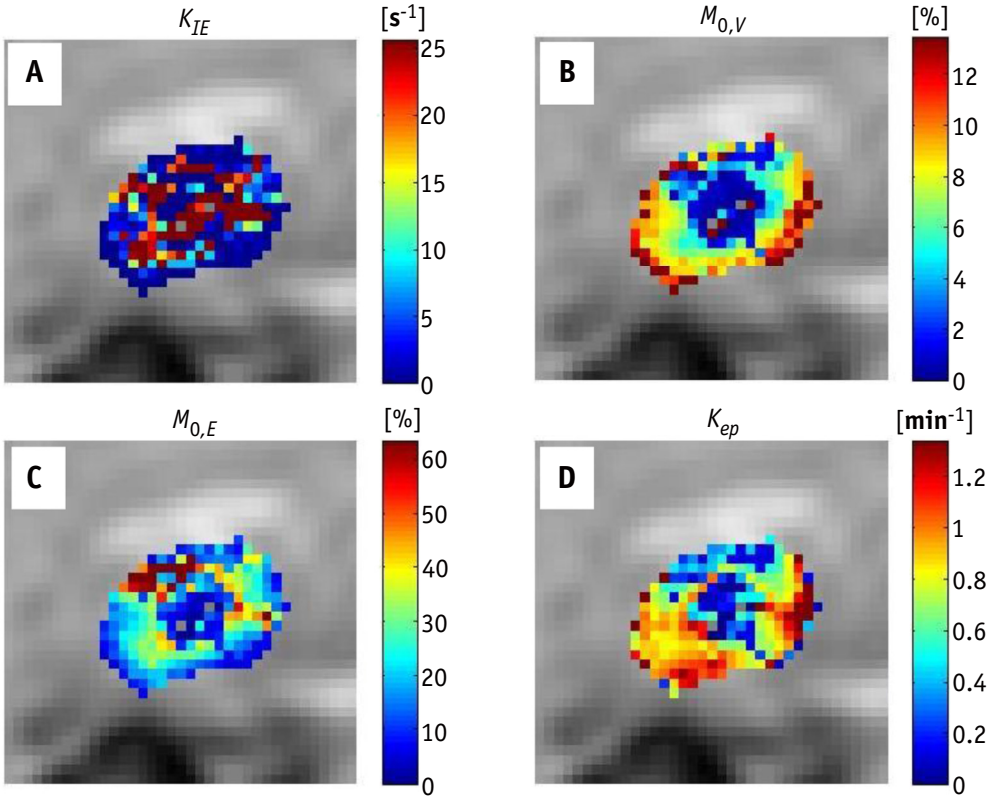

Fig. 3. The parametric maps of all 4 independent model parameters overlaid on the dynamic contrast-enhanced MR image: (A) Intracellular–extracellular water exchange rate constant, k_{IE} [s^{-1}], (B) the vascular compartment volume fraction, $M_{0,V}$, (C) the extracellular–extravascular compartment volume fraction, $M_{0,E}$, and (D) efflux rate constant k_{ep} [min^{-1}], calculated for the sample dynamic contrast-enhanced MRI data that was shown in Figure 2 (compartment volume fractions represent percentage of the voxel that correspond to each compartment and are unitless).

parameter (between pretreatment and 1 week after treatment scans), as well as tumor volume change (at 1-week and 1-month posttreatment scans). It also shows the statistical significance (via P value) of each parameter separating the PR group from the rest (SD + PD). Among model parameters, the intracellular–extracellular water exchange rate constant, k_{IE}, and extracellular–extravascular compartment volume fraction, $M_{0,E}$, separated the PR patients with statistically significant differences.

Figure 4 presents the change in each model parameter (between 1-week posttreatment and pretreatment scans) plotted versus the relative change in tumor volume (between 1-month posttreatment and pretreatment scans). These plots show high correlations for intracellular–extracellular water exchange rate constant, k_{IE} ($R=-0.76$, $P<.001$), and extracellular–extravascular volume fraction, $M_{0,E}$ ($R=-0.62$, $P=.005$). However, for efflux rate constant, k_{ep} ($R=-0.09$, $P=.72$), and vascular compartment volume

Table 2 Average and standard deviation of change in parameters between pretreatment and 1-week posttreatment scans and tumor volume change at 1 week and 1 month of patients in each cohort

Parameter	Partial response (PR)	Stable disease (SD)	Progressive disease (PD)	P (PR vs SD + PD)
No. of patients	12	3	4	-
ΔVolume (cm^3) (1 mo)	**−1.2 ± 0.9**	**−0.3 ± 0.1**	**0.5 ± 0.5**	.001
ΔVolume (cm^3) (1 wk)	0.3 ± 1.3	0.2 ± 0.2	0.2 ± 0.3	.4
Δk_{IE} (s^{-1})	**3.7 ± 2.9**	**−2.8 ± 1.2**	**−2.3 ± 1.1**	<.001
$\Delta M_{0,E}$ (%)	**11 ± 17**	**−6 ± 5**	**−9 ± 12**	.01
$\Delta M_{0,V}$ (%)	−0.7 ± 5.6	−0.7 ± 3.2	0.3 ± 4.4	.9
Δk_{ep} (min^{-1})	0.07 ± 0.63	−0.37 ± 0.41	0.0 ± 0.66	.7

Bold indicates $P<.05$ that is considered statistically significant.

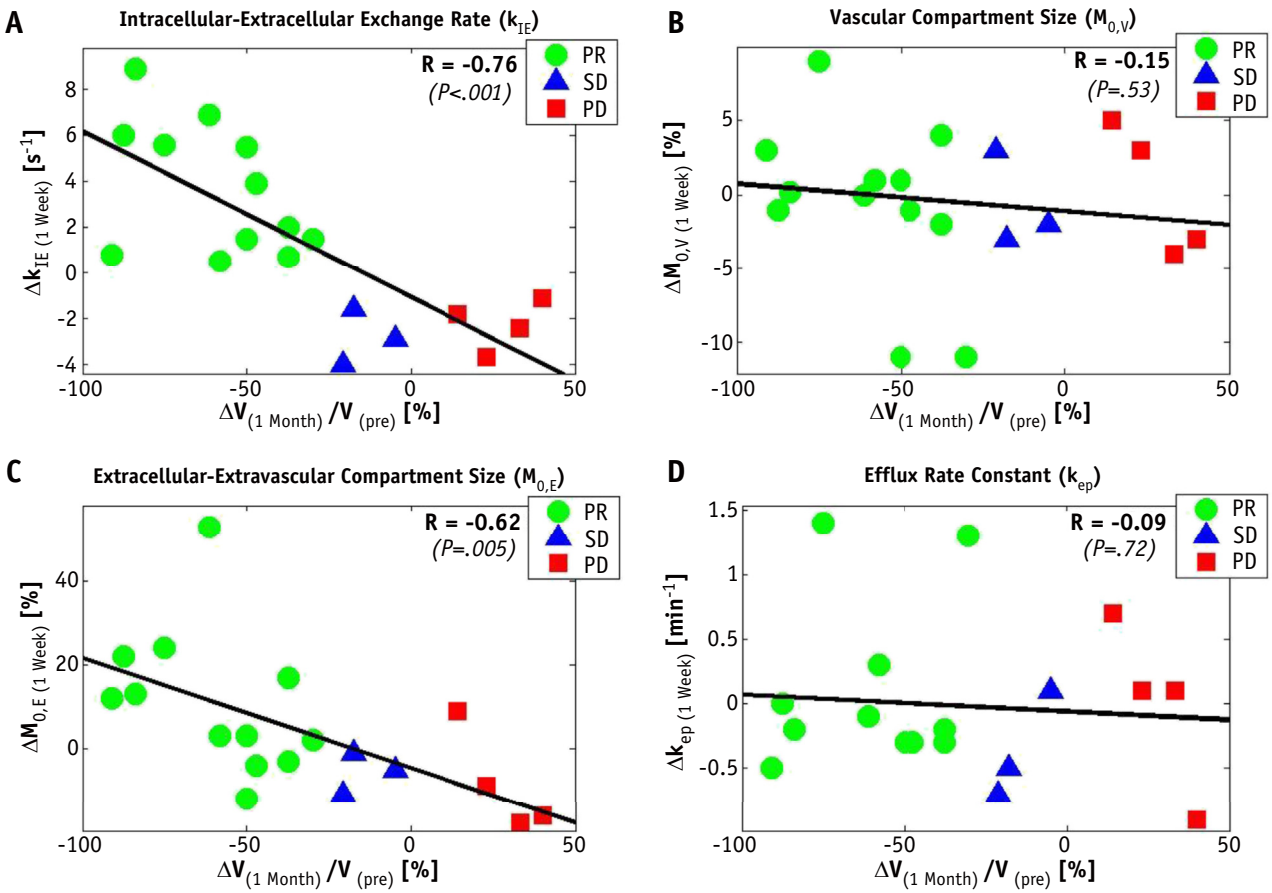

Fig. 4. The change in the model parameters (mean value over tumor region) between the pretreatment and 1-week posttreatment scans versus the relative change in tumor volume between the pretreatment and 1-month posttreatment scans for (A) the intra−extracellular water exchange rate constant, k_{IE}, (B) the vascular compartment volume fraction, $M_{0,V}$, (C) the extracellular−extravascular compartment volume fraction, $M_{0,E}$, and (D) the efflux rate constant k_{ep}. The subscript "pre" represents the pretreatment value of the parameter. Partial response (PR), stable disease (SD), and progressive disease (PD) patients are represented with circles, triangles, and squares, respectively.

fraction, $M_{0,V}$ ($R=-0.15$, $P=.53$), there was no correlation, and thus these parameters were unable to separate the 3 patient groups.

Moreover, relative change in tumor volume at 1 week ($R=0.01$, $P=.9$), and change in longitudinal relaxation rate, R_{10}, of the tumor ($R=-0.39$, $P=.089$) did not correlate with tumor volume change at 1 month (not shown).

Discussion

The objective of this prospective study was to establish whether quantitative MRI can evaluate the response of brain metastases to SRS within the first week after treatment (as compared with clinical evaluation by tumor volume measurement at later time points). Differentiation of responders from nonresponders early after the treatment is useful in clinical practice. Nonresponders can be considered for salvage treatments, such as surgery or reirradiation, earlier and avoid morbidity associated with delayed identification of PD. Moreover, correlating early changes in MRI parameters to tumor volume change at 1 month provides additional insight into disease progression and could potentially be useful in managing patients.

In this study the 1-month time point was chosen for response assessment because it commonly is the first time point after treatment to assess response. It has also been shown to be strongly associated with long-term control of the brain metastasis (32). Moreover, a blinded oncologist evaluated the long-term response of the patients in this study. The evaluation was performed by assessing the pretreatment tumor size and its size at all available follow-up scans (longer than 3 months after treatment). This long-term response evaluation was feasible for 17 of 19 cases (no long-term follow-up was available for 2 cases). In all but 1 case the long-term follow-up confirmed the assessment at 1 month, and only 1 case that was classified as having PR showed progression at follow-up MRI 6 months after treatment.

Tumor volume at 1 week after treatment increased in 6 of 12 PR patients, in all SD patients, and in 3 of 4 PD patients. There was no statistically significant difference

between tumor volume change at 1 week for different patient groups (Table 2), and there was no correlation between tumor volume change at 1 week and at 1 month after treatment ($R=0.01$, $P=.9$), demonstrating that this parameter is not a reliable early biomarker of response to SRS.

Early changes in intracellular to extracellular water exchange rare constant, k_{IE}, (within 1 week after treatment) were capable of predicting tumor behavior in patients with PR and in patients with SD and PD. As reported in Table 2, there was a statistically significant difference between the changes in the intra−extracellular exchange rate constant, k_{IE}, for the PR group compared with the SD and PD groups (1 week after treatment), and this parameter could separate the PR patients from the other 2 groups. However, there was no difference between PD and SD cohorts. There was also a high negative correlation ($R=-0.76$, $P<.001$) between the early changes in the intra−extracellular exchange rate constant, k_{IE}, and relative tumor volume change 1 month after treatment (Fig. 4).

The water exchange rate constant, k_{IE}, increased in PR patients and decreased in SD and PD patients (suggesting the treatment was unsuccessful in inducing sufficient apoptosis in SD and PD). This trend was expected as a result of increased surface-to-volume ratio in cells undergoing apoptosis and, to a lesser extent, increased membrane permeability (10) in responding patients (PR). Additionally, for the 1 case that showed PR at 1 month but progressed at long term, there was a small change in k_{IE} at 1 week ($\Delta k_{IE} = 0.6[s^{-1}]$), suggesting that by selecting a different cut-off threshold, this case could also be accurately classified. These results demonstrated that the intra−extracellular water exchange rate constant, k_{IE}, could be used as an early biomarker for treatment response of brain metastasis to SRS.

In a majority of cases there were statistically significant changes in the extracellular−extravascular volume fractions, $M_{0,E}$, 1 week after treatment. As reported in Table 2, this parameter was capable of separating the PR group from the SD and PD groups, and as shown in Figure 4 there was a relatively high correlation between early changes in this volume fraction and relative change in tumor volume 1 month after treatment ($R=-0.62$, $P=.005$). For the 1 case with PR at 1 month and progression at long term, the change in extracellular−extravascular volume fractions, $M_{0,E}$, at 1 week was negative ($\Delta M_{0,E} = -3[\%]$), which is similar to the PD group. These results demonstrate that $M_{0,E}$ is also a promising candidate for assessing tumor response to SRS.

Stereotactic radiosurgery is expected to have antivascular effects (4, 33-35), with severe vascular damage resulting in reduced blood perfusion. Such changes usually take place at early stages after treatment (1 week after treatment) (34, 35). As expected, in most cases there was a statistically significant change in the vascular compartment volume fraction 1 week after treatment. However, there was not a distinct trend in its changes, and it was not capable of separating the patient groups (Table 2).

Moreover, early change in the efflux rate constant, k_{ep}, did not correlate with tumor response, and this parameter was unable to predict tumor behavior in different patient groups (Table 2). There was also no correlation between early changes in the efflux rate constant and relative change in tumor volume 1 month after SRS ($R=-0.09$, $P = .72$).

It is expected that approximately 20% to 25% of patients with brain metastasis do not respond to SRS 1 month after treatment (32, 36). In our patient population of 19 patients, 4 patients were classified as having PD, which demonstrated that our patient population was a representative group. However; a larger cohort of patients is required to confirm the relationship between the early changes in intra−extracellular water exchange rate constant, k_{IE}, and tumor volume at 1 month after treatment with higher confidence.

References

1. Andrews DW, Scott CB, Sperduto PW, et al. Whole brain radiation therapy with or without stereotactic radiosurgery boost for patients with one to three brain metastases: Phase III results of the RTOG 9508 randomised trial. *Lancet* 2004;363:1665-1672.
2. Chang EL, Wefel JS, Hess KR, et al. Neurocognition in patients with brain metastases treated with radiosurgery or radiosurgery plus whole-brain irradiation: A randomised controlled trial. *Lancet Oncol* 2016; 10:1037-1044.
3. Lin NU, Lee EQ, Aoyama H, et al. Response assessment criteria for brain metastases: Proposal from the RANO group. *Lancet Oncol* 2015; 16:e270-e278.
4. Park HJ, Griffin RJ, Hui S, et al. Radiation-induced vascular damage in tumors: Implications of vascular damage in ablative hypofractionated radiotherapy (SBRT and SRS). *Radiat Res* 2012;177:311-327.
5. Coolens C, Driscoll B, Foltz W, et al. Tumour response assessment using volumetric DCE-CT and DCE-MRI in metastatic brain cancer patients. Presented at the 23rd Annual Meeting and Exhibition of the International Society for Magnetic Resonance in Medicine, May 30-June 5, 2015, Toronto, ON, Canada.
6. Cabrera AR, Cuneo KC, Desjardins A, et al. Concurrent stereotactic radiosurgery and bevacizumab in recurrent malignant gliomas: A prospective trial. *Int J Radiat Oncol Biol Phys* 2013;86:873-879.
7. Mehrabian H, Martel AL, Le Floc'h J, et al. Quantification of water exchange between intravascular and extravascular compartments using independent component analysis. Presented at the 23rd Annual Meeting and Exhibition of the International Society for Magnetic Resonance in Medicine, May 30-June 5, 2015, Toronto, ON, Canada.
8. Thoeny HC, Ross BD. Predicting and monitoring cancer treatment response with DW-MRI. *J Magn Reson Imaging* 2010;32:2-16.
9. Ellis P, Smith I, McCarthy K, et al. Preoperative chemotherapy induces apoptosis in early breast cancer. *Lancet* 1997;349:849.
10. Bailey C, Giles A, Czarnota GJ, et al. Detection of apoptotic cell death in vitro in the presence of Gd-DTPA-BMA. *Magn Reson Med* 2009; 62:46-55.
11. Bailey C, Moosvi F, Stanisz GJ. Mapping water exchange rates in rat tumor xenografts using the late-stage uptake following bolus injections of contrast agent. *Magn Reson Med* 2014;71:1874-1887.
12. Donahue KM, Burstein D, Manning WJ, et al. Studies of Gd-DTPA relaxivity and proton exchange rates in tissue with implications for MR imaging of regional myocardial perfusion. *Magn Reson Med* 1994;32:66-76.

13. Darzynkiewicz Z, Juan G, Li X, et al. Cytometry in cell necrobiology: Analysis of apoptosis and accidental cell death (necrosis). *Cytometry* 1997;27:1-20.
14. Springer CS Jr., Li X, Tudorica LA, et al. Intratumor mapping of intracellular water lifetime: Metabolic images of breast cancer? *NMR Biomed* 2014;27:760-773.
15. Sobol WT, Jackels SC, Cothran RL, et al. NMR spin-lattice relaxation in tissues with high concentration of paramagnetic contrast media: Evaluation of water exchange rates in intact rat muscle. *Med Phys* 1991;18:243-250.
16. Buckley DL, Kershaw LE, Stanisz GJ. Cellular-interstitial water exchange and its effect on the determination of contrast agent concentration in vivo: Dynamic contrast-enhanced MRI of human internal obturator muscle. *Magn Reson Med* 2008;60:1011-1019.
17. Yankeelov TE, Rooney WD, Li X, et al. Variation of the relaxographic "shutter-speed" for transcytolemmal water exchange affects the CR bolus-tracking curve shape. *Magn Reson Med* 2003;50:1151-1169.
18. Landis CS, Li X, Telang FW, et al. Equilibrium transcytolemmal water-exchange kinetics in skeletal muscle in vivo. *Magn Reson Med* 1999;42:467-478.
19. Yankeelov TE, Rooney WD, Huang W, et al. Evidence for shutter-speed variation in CR bolus-tracking studies of human pathology. *NMR Biomed* 2005;18:173-185.
20. Tofts PS, Brix G, Buckley DL, et al. Estimating kinetic parameters from dynamic contrast-enhanced T1-weighted MRI of a diffusable tracer: Standardized quantities and symbols. *J Magn Reson Imaging* 1999;10:223-232.
21. Mehrabian H, Chopra R, Martel AL. Calculation of intravascular signal in dynamic contrast enhanced-MRI using adaptive complex independent component analysis. *IEEE Trans Med Imaging* 2013;32:699-710.
22. Mehrabian H, Chandrana C, Pang I, et al. Arterial input function calculation in dynamic contrast-enhanced MRI: An in vivo validation study using co-registered contrast-enhanced ultrasound imaging. *Eur Radiol* 2012;22:1735-1747.
23. Mehrabian H, Pang I, Chopra R, et al. An adaptive complex independent component analysis to analyze dynamic contrast enhanced-MRI. Presented at the IEEE 9th International Symposium on Biomedical Imaging, May 2-5, 2012, Barceloca, Spain.
24. Mehrabian H, Da Rosa M, Haider MA, et al. Pharmacokinetic analysis of prostate cancer using independent component analysis. *Magn Reson Imaging* 2015;33:1236-1245.
25. McConnell HM. Reaction rates by nuclear magnetic resonance. *J Chem Phys* 1958;28:430-431.
26. Naish JH, Kershaw LE, Buckley DL, et al. Modeling of contrast agent kinetics in the lung using T1-weighted dynamic contrast-enhanced MRI. *Magn Reson Med* 2009;61:1507-1514.
27. Pintaske J, Martirosian P, Graf H, et al. Relaxivity of gadopentetate dimeglumine (Magnevist), gadobutrol (Gadovist), and gadobenate dimeglumine (MultiHance) in human blood plasma at 0.2, 1.5, and 3 Tesla. *Invest Radiol* 2006;41:213-221.
28. Zhang X, Petersen ET, Ghariq E, et al. In vivo blood T1 measurements at 1.5 T, 3 T, and 7 T. *Magn Reson Med* 2013;70:1082-1086.
29. Barsky D, Putz B, Schulten K. Theory of heterogeneous relaxation in compartmentalized tissues. *Magn Reson Med* 1997;37:666-675.
30. Chavez S, Stanisz GJ. A novel method for simultaneous 3D B1 and T1 mapping: The method of Slopes (MoS). *NMR Biomed* 2012;25:1043-1055.
31. Chavez S. Optimized method of Slopes (MoS) produces robust and efficient 3D B1-corrected T1 maps. Presented at the 23rd Annual Meeting and Exhibition of the International Society for Magnetic Resonance in Medicine, May 5-11, 2012, Melbourne, Australia.
32. Sharpton SR, Oermann EK, Moore DT, et al. The volumetric response of brain metastases after stereotactic radiosurgery and its post-treatment implications. *Neurosurgery* 2014;74:9-15.
33. Clement JJ, Song CW, Levitt SH. Changes in functional vascularity and cell number following X-irradiation of a murine carcinoma. *Int J Radiat Oncol Biol Phys* 1976;1:671-678.
34. Solesvik OV, Rofstad EK, Brustad T. Vascular changes in a human malignant melanoma xenograft following single-dose irradiation. *Radiat Res* 1984;98:115-128.
35. Bussink J, Kaanders JH, Rijken PF, et al. Changes in blood perfusion and hypoxia after irradiation of a human squamous cell carcinoma xenograft tumor line. *Radiat Res* 2000;153:398-404.
36. Kim WH, Kim DG, Han JH, et al. Early significant tumor volume reduction after radiosurgery in brain metastases from renal cell carcinoma results in long-term survival. *Int J Radiat Oncol Biol Phys* 2012;82:1749-1755.